

Testing Statistical Isotropy in Cosmic Microwave Background Polarization maps

Pranati K. Rath,^{1,2*} Pramoda Kr. Samal,^{3†} Srikanta Panda³, Debesh D. Mishra⁴, Pavan K. Aluri^{5,6}

¹*Institute of High Energy Physics, Chinese Academy of Sciences, Beijing 100049, China*

²*Theoretical Physics Center for Science Facilities, Chinese Academy of Sciences, Beijing 100049, China*

³*Department of Physics, Utkal University, Bhubaneswar, Odisha, 751004, India*

⁴*State Key Laboratory of Advanced Technology for Materials Synthesis and Processing, Wuhan University of Technology, Wuhan 430070, China*

⁵*Korea Institute for Advanced Study, Quantum Universe Center, 85 Hoegi-ro, Dongdaemun-gu, Seoul - 02455, Republic of Korea*

⁶*Korea Astronomy and Space Science Institute, 776 Daedeokdae-ro, Yuseong-gu, Daejeon - 305348, Republic of Korea*

Accepted XXX. Received YYY; in original form ZZZ

ABSTRACT

We apply our symmetry based *Power tensor* technique to test conformity of PLANCK Polarization maps with statistical isotropy. On a wide range of angular scales ($l = 40 - 150$), our preliminary analysis detects many statistically anisotropic multipoles in foreground cleaned full sky PLANCK polarization maps viz., COMMANDER and NILC. We also study the effect of residual foregrounds that may still be present in the galactic plane using both common UPB77 polarization mask, as well as the individual component separation method specific polarization masks. However some of the statistically anisotropic modes still persist, albeit significantly in NILC map. We further probed the data for any coherent alignments across multipoles in several bins from the chosen multipole range.

Key words: cosmic microwave background - polarization - data analysis

1 INTRODUCTION

The standard cosmological model is based on the postulate that the universe is homogeneous and isotropic on large distance scales. However, there exist many observations which suggest that this postulate is violated. The first indication of statistical anisotropy came from the analysis of radio polarization from distant radio galaxies (Birch 1982; Jain & Ralston 1999; Jain et al. 2004). Those authors found that the polarization offsets, after eliminating the effect of Faraday rotation show a dipole pattern on the sky and the dipole axis points towards the Virgo cluster of galaxies, very close to the direction of the CMB dipole (Jain & Ralston 1999). The optical polarizations of distant quasars shows alignment over very large distance scales (Hutsemekers 1998; Hutsemekers & Lamy 2001). The distance scale of alignment is found to be of the order of 1 Gpc (Jain et al. 2004), and the axis again points close to the CMB dipole axis. The CMB quadrupole and octopole also indicates a preferred direction pointing towards the Virgo cluster (Copi et al. 2004; Ralston & Jain 2004; de Oliveira-Costa et al. 2004; Schwarz et al. 2004; Bielewicz et al. 2005; Samal et al. 2008). This phe-

nomenon where several axes from various data sets broadly indicate the same direction has been called *Virgo alignment puzzle* (Jain et al. 2004). Besides the Virgo alignment, there also exists statistically significant signals of anisotropy in CMB temperature data viz., hemispherical power asymmetry (Eriksen et al. 2004; Prunet et al. 2005; Hansen et al. 2009; Hanson & Lewis 2009; Hoftuft et al. 2009; Rath & Jain 2013; Akrami et al. 2014; Aiola et al. 2015; Rath et al. 2015), parity asymmetry (Land & Magueijo 2005; Kim & Naselsky 2010, 2011; Aluri & Jain 2012; Zhao 2014; Aluri et al. 2017) and a region of significant temperature decrement known as cold spot (Vielva et al. 2004; Cruz et al. 2005, 2006, 2008; Zhao 2013; Nadathur et al. 2014; Aluri & Rath 2016).

Large angle CMB anisotropies have been a subject of several studies in the cosmology literature - see for example Bennett et al. (2011); Planck Collaboration XXIII (2013); Planck Collaboration XVI (2016) for an evaluation of some of the prominent large angle anomalies by WMAP and PLANCK collaborations. General methods have been developed to test any violation of statistical isotropy in the CMB data (Hajian & Souradeep 2003, 2006; Copi et al. 2004, 2006; Samal et al. 2008, 2009). In Samal et al. (2008, 2009), a symmetry based method for testing the isotropy of CMB temperature data called *Power tensor* was proposed. The method is based on identifying invariants corresponding to

* Email: pranati@ihep.ac.cn

† Email: pksamal@iopb.res.in

each multipole using the Power tensor matrix defined as

$$A_{ij}(l) = \frac{1}{l(l+1)(2l+1)} \sum_{m,m'} a_{lm}^*(J_i J_j)_{mm'} a_{lm'}. \quad (1)$$

Here $J_i (i = 1, 2, 3)$ are the angular momentum operators in spin- l representation. The sum of the three eigenvalues reproduce the usual angular power spectrum, C_l . Statistical nature of CMB anisotropies lead to fluctuations in the eigenvalues of Power tensor about their expected value of $C_l/3$ in a given realization. The significance of any deviation from isotropy is measured using an invariant combination of normalized eigenvalues of the Power tensor called *Power entropy* (Samal et al. 2008, 2009; Rath & Samal 2015).

In this paper, we probe statistical anisotropy, if any, in the PLANCK CMB polarization data using our symmetry based method, and its possible relation to the existing anomalies of CMB temperature sky. A violation of statistical isotropy can arise due to a variety of sources, for example, from residual contamination due to foregrounds, beam systematics, inhomogeneous noise, etc. Here we do not make any attempt to find the exact cause of breakdown of isotropy, if found eventually in our analysis.

The paper is organized as follows. In section 2, we briefly review CMB polarization convention. Then the statistics used to analyze the data are defined in section 3. The data used in the present work is described in section 4, and our results are discussed in section 5. There, we first present the results from analyzing full sky PLANCK CMB polarization maps. Then we go on to discuss the effect of foreground residuals if any on our results by employing different galactic masks, also provided by PLANCK team. We also present results from our tests for any coherent alignments among various multipoles. Finally, the work is summarized in section 6.

2 CMB POLARIZATION MAPS

The full sky CMB signal is described by Stokes parameters I , Q , U and V . The Stokes parameter I represents the temperature field, and the Stokes parameters (Q, U) represent the linear polarization field. In the standard model of cosmology, the CMB temperature fluctuations are expected to be an isotropic Gaussian random field, and are conventionally expanded in terms of the spherical harmonics as

$$T(\hat{n}) = \sum_{lm} a_{lm} Y_{lm}(\hat{n}), \quad (2)$$

where a_{lm} are the coefficients of expansion. The CMB polarization is induced by Thomson scattering of CMB photons at the last scattering surface. The WMAP and PLANCK teams provided maps of CMB polarization in terms of the Stokes parameters Q and U , though with low signal to noise ratio (SNR). The Stokes parameter V , which describes circular polarization is ignored as it cannot be generated through Thomson scattering.

From now onwards we use the notation of Zaldarriaga & Seljak (1997) for the polarization fields. Instead of the Stokes parameters Q and U , it is useful to employ special combinations of these parameters as $X_{\pm} = Q \pm iU$, which transform as spin-2 fields under coordinate rotation. Under a rotation by an angle ϕ of the co-ordinate frame in which the

polarization vector is defined, the combinations X_{\pm} behave as spin ± 2 fields viz.,

$$(Q \pm iU)'(\hat{n}) = e^{\mp 2i\phi} (Q \pm iU)(\hat{n}). \quad (3)$$

Analogous to the expansion of temperature field in terms of the spherical harmonics, $Y_{lm}(\hat{n})$, there also exists a set of spin- s spherical harmonics ${}_s Y_{lm}(\hat{n})$, in terms of which one can expand a spin- s function on a sphere. We can, therefore, expand $X_{\pm}(\hat{n}) = (Q \pm iU)(\hat{n})$ in terms of the spin-2 spherical harmonics as

$$X_{\pm}(\hat{n}) = \sum_{lm} a_{\pm 2, lm} {}_{\pm 2} Y_{lm}(\hat{n}). \quad (4)$$

Owing to the real nature of Q and U parameters, the expansion coefficients satisfy the condition : $a_{-2, lm}^* = a_{2, l-m}$. Using the following identities

$$\bar{\delta} {}_s Y_{lm} = \sqrt{(l-s)(l+s+1)} {}_{s+1} Y_{lm}, \quad (5)$$

$$\bar{\delta} {}_s Y_{lm} = -\sqrt{(l+s)(l-s+1)} {}_{s-1} Y_{lm}. \quad (6)$$

for the spin raising and lowering operators : $\bar{\delta}$ and $\bar{\delta}$, spin-0 objects can be constructed from spin-2 fields as

$$\bar{\delta}^2(Q + iU)(\hat{n}) = \sum_{lm} \sqrt{\frac{(l+2)!}{(l-2)!}} a_{2, lm} Y_{lm}(\hat{n}), \quad (7)$$

$$\bar{\delta}^2(Q - iU)(\hat{n}) = \sum_{lm} \sqrt{\frac{(l+2)!}{(l-2)!}} a_{-2, lm} Y_{lm}(\hat{n}). \quad (8)$$

Finally, the rotationally invariant polarization fields are defined as

$$\begin{aligned} \tilde{E}(\hat{n}) &= -\frac{1}{2} [\bar{\delta}^2(Q + iU) + \bar{\delta}^2(Q - iU)] \\ &= \sum_{lm} \tilde{a}_{lm}^E Y_{lm}(\hat{n}), \end{aligned} \quad (9)$$

$$\begin{aligned} \tilde{B}(\hat{n}) &= -\frac{1}{2i} [\bar{\delta}^2(Q + iU) - \bar{\delta}^2(Q - iU)] \\ &= \sum_{lm} \tilde{a}_{lm}^B Y_{lm}(\hat{n}) \end{aligned} \quad (10)$$

where $\tilde{a}_{lm}^{E/B} = \sqrt{(l+2)!/(l-2)!} a_{lm}^{E/B}$, and a_{lm}^E and a_{lm}^B are the spherical harmonic coefficients of “E-mode” and “B-mode” polarization fields. Note that often E/B harmonic coefficients (and consequently the E/B fields) are defined without the extra $\sqrt{(l+2)!/(l-2)!}$ factor. These E/B spherical harmonic coefficients are given by linear combinations of spin-2 spherical harmonic coefficients of Stokes Q/U polarization fields as

$$a_{lm}^E = -\frac{1}{2} (a_{2, lm} + a_{-2, lm}), \quad (11)$$

$$a_{lm}^B = -\frac{1}{2i} (a_{2, lm} - a_{-2, lm}). \quad (12)$$

Here we restrict our attention to the $E(\hat{n})$ field (ie., a_{lm}^E coefficients), to study statistical isotropy of PLANCK polarization maps.

3 STATISTICS

The angular orientation of each mode is given by a unique orthonormal frame $e_k^\alpha(l)$ and rotationally invariant singular

values $\Lambda_\alpha(l)$ of the Power tensor, $A(l)$, defined in Eq. (1). Here $k = 1, 2, 3$ denote the components of the frame vector $\mathbf{e}^\alpha(l)$ and $\alpha = 1, 2, 3$ stands for the singular value index. In terms of these quantities, the Power tensor matrix for each multipole ‘ l ’ can be expressed as

$$A_{ij}(l) = \sum_{\alpha} e_i^\alpha (\Lambda^\alpha)^2 e_j^{\alpha*}. \quad (13)$$

We do not explicitly display the index l when it is obvious. We refer to the eigenvector corresponding to the largest eigenvalue of the Power tensor as *principal eigenvector* (PEV), and is taken to be the anisotropy axis of that multipole. The preferred direction represented by a PEV of any multipole is quantified by parametrizing the dispersion of eigenvalues using *Power entropy* that is defined as

$$S_p(l) = - \sum_{\alpha} \lambda^\alpha \log(\lambda^\alpha) \quad (14)$$

where $\lambda^\alpha = (\Lambda^\alpha)^2 / \sum_{\beta} (\Lambda^\beta)^2$. In the ideal case of isotropy, where all the three eigenvalues are degenerate and equal to $C_l/3$, we have maximum Power entropy, $S_p \rightarrow \log(3)$. In the case of a *pure state*, where one of the eigenvalues contains the total power and other two vanishes, it leads to vanishing Power entropy, $S_p \rightarrow 0$. So for our observational data, the range of Power entropy is $0 \leq S_p \leq \log(3)$. Hence low Power entropy in data, compared to consistently generated concordance model simulations, is a measure of isotropy violation in the data.

Now, a common alignment vector using PEVs for a set of multipoles or range of multipoles can be calculated using what is called an *Alignment entropy*, defined by

$$S_X = -\text{Tr}(\rho_X \log(\rho_X)), \quad (15)$$

where $\rho_X = X/\text{Tr}(X)$ is the normalized 3×3 matrix ‘ X ’ that is referred to as *Alignment tensor*. It is given by

$$X_{ij} = \sum_{l_{min}}^{l_{max}} e^i(l) e^j(l), \quad (16)$$

where $\mathbf{e}(l)$ is the PEV of a multipole, l . $\text{Tr}(X)$ denotes trace of X . An unusually low value of S_X compared to $\log(3)$ confirms violation of isotropy over a wider multipole range. We note that the Power entropy and the Alignment entropy are independent of each other.

The significance of statistical anisotropy is determined by comparing the data statistic value with that of simulations and the significance is quoted by the P -value. A P -value is defined as the probability that a random realization may yield a statistic smaller than that seen in data. The effective probability for a collection of PEVs with respective P -values less than a reference probability ‘ \mathbb{P} ’, is estimated using the binomial distribution of *pass* and *fail* outcomes. The probability to encounter k instances of passing defined by probability \mathbb{P} in n trials is

$$f(k|n, \mathbb{P}) = \frac{\mathbb{P}^k (1 - \mathbb{P})^{n-k} n!}{(n - k)! k!} \quad (17)$$

In assessing many P -values, we report the cumulative binomial probabilities as

$$f(k \geq k_* | n, \mathbb{P}) = \sum_{k=k_*}^n f(k|n, \mathbb{P}) \quad (18)$$

which is the probability to see k_* or more instances of passing among n trials defined by a threshold probability \mathbb{P} .

4 DATA USED

The PLANCK team has provided four foreground reduced CMB polarization maps referred to as COMMNDER, NILC, SMICA and SEVEM (Planck Collaboration IX 2016) maps, named after the component separation procedure used. Out of these four, we study only the COMMNDER and NILC as they are full sky maps which are suitable for our study. The other clean CMB maps viz., SMICA and SEVEM polarization solutions have a portion of the sky removed, particularly in the galactic plane. Hence we will not use them in our analysis. All these cleaned polarization CMB maps were estimated using all the frequency channels aboard PLANCK that are sensitive to polarization (from 30 to 353 GHz). Due to the presence of significant noise in the polarization maps and also due to the possible residual foregrounds that may still be present even after cleaning, any signature of large scale isotropy breakdown has to be interpreted with care. Here we use half-ring half-difference (HRHD) maps (Planck Collaboration IX 2016) as noise proxy in our analysis. The publicly available polarization maps don’t include low- l up to $l = 40$ owing to systematics (Planck Collaboration IX 2016). Consequently, we only analyze multipoles $l \geq 40$. As noise contribute dominantly to the polarization maps from PLANCK at high- l , we restrict our analysis up to $l = 150$.

To start with, we extract the E -mode polarization map from the full sky Stokes Q and U maps from PLANCK available at a HEALPix (Gorski et al. 2005) resolution of $N_{side} = 1024$ and have a beam resolution given by a Gaussian beam of $FWHM = 10'$ (arcmin). We first analyze the full sky COMMNDER and NILC foreground cleaned PLANCK E -mode polarization maps thus obtained. Subsequently we generate foreground-residual minimized full sky CMB E -mode data maps by following the procedure described in Samal et al. (2010); Rath et al. (2013, 2015). For the purposes of masking, we use the common polarization mask $UPB77$, as well as the polarization masks specific to each component separation method employed by PLANCK (Planck Collaboration IX 2016). These masks are shown in Fig. (1). The common polarization mask, $UPB77$ cover $\approx 77\%$ of the sky whereas the COMMANDER and NILC polarization masks cover $\approx 83\%$ and 96% of the sky respectively. From now on we abbreviate the COMMANDER polarization mask as $PMCMDR$ and the NILC polarization mask as $PMNILC$.

A full sky CMB E -mode data map with minimized residual foregrounds is generated following the steps listed below :

(i) We first generate a full sky CMB IQU random realization using the best fit theoretical angular power spectrum (C_l^{th}). The best fit C_l^{th} are generated using PLANCK 2015 cosmological parameters (Planck Collaboration XI 2016; Planck Collaboration XIII 2016) as input to CAMB software (Lewis et al. 2000; Howlett et al. 2012). The values of cosmological parameters from PLANCK 2015 results that we used are baryon matter density $\Omega_b h^2 = 0.0222$, cold dark matter density $\Omega_c h^2 = 0.1203$, neutrino energy density $\Omega_\nu h^2 = 0.00064$, cosmological constant density fraction $\Omega_\Lambda = 0.6823$, Hubble parameter H_0 with $h = 0.6712$, scalar spectral index of the primordial power spectrum $n_s = 0.96$, amplitude of primordial power spectrum $A_s = 2.09 \times 10^{-9}$, and reionization optical depth $\tau = 0.078$. The best fit the-

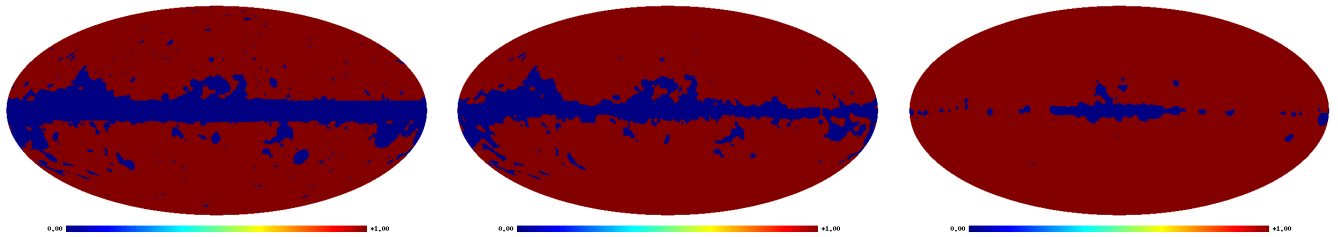


Figure 1. *Left* : UPB77 common polarization analysis mask, *Middle* : COMMANDER polarization map (PMCMR), *Right* : NILC polarization mask (PMNILC). All these masks are available at $N_{side} = 1024$.

oretical angular power spectrum, C_l^{th} , thus obtained from CAMB using these parameters, is employed to generate random realizations of CMB sky using HEALPix. A CMB IQU map is generated with a Gaussian beam of $FWHM = 10'$ (arcmin) at $N_{side} = 1024$.

(ii) A cosine filter is then applied on the simulated CMB IQU random realization obtained in step (i), to remove the large angular scales following [Planck Collaboration IX \(2016\)](#). The cosine filter is defined as

$$w_l = \begin{cases} 0, & l < l_1 \\ \frac{1}{2} \left[1 - \cos \left(\pi \frac{l-l_1}{l_2-l_1} \right) \right], & l_1 \leq l \leq l_2 \\ 1, & l_2 < l, \end{cases} \quad (19)$$

where $l_1 = 20$ and $l_2 = 40$.

(iii) The IQU noise proxies viz., the HRHD maps corresponding to COMMANDER/NILC component separation method are added to the filtered CMB IQU realization obtained in step (ii). Note that the cosine filter given by Eq. (19) is already applied to the HRHD polarization data maps that are made publicly available. This results in a random CMB realization with noise levels similar to data.

(iv) Now, the inverse of polarization masks shown in Fig. (1) are applied to the random CMB IQU realization added with an HRHD map. By doing so, the resultant map will have signal only in the galactic region (and few other regions), with rest of the sky set to zero. Next, we apply the polarization masks of Fig. (1), as they are, on the CMB data IQU map to remove the potentially contaminated galactic region. Finally the two pieces that have complementary regions masked are added together to construct a full sky CMB IQU data map at $N_{side} = 1024$.

(v) Subsequently, we derive the E -mode polarization map from this composite data IQU map at $N_{side} = 1024$.

Thus we have effectively minimized the residual contamination in the data CMB polarization map.

Due to random filling of the masked regions, one will get a (slightly) different value for the statistic, compared to the *true* sky. Hence our data statistic is taken as average value of the same quantity derived from 100 such *filled* full sky COMMANDER and NILC IQU maps.

The significance of isotropy violation is estimated by comparing the (average) data statistic value with 4000 random CMB realizations (added with HRHD noise maps). Since we have different HRHD maps for COMAMNDER and NILC maps, we generate two sets of 4000 random realizations. Simulations of CMB IQU maps with noise levels similar to data are generated following step (i) - (iii) described above. We then extract the E -mode polarization

map from these realistic IQU maps. We note that the temperature realizations generated here are only a by-product and have no use for us. So any operation like masking or filtering performed on I map, together with Q and U maps, has no relevance to our study.

5 RESULTS

First we analyze the *full sky* PLANCK E -mode polarization maps as obtained from cleaned CMB data IQU map. Later we use the *filled* data maps to understand the effect of residual contamination that may still be present in the recovered CMB sky. Recall that in order to minimize likely foreground bias on our results, we filled the masked regions shown in Fig. (1), with a filtered random isotropic realization added with an HRHD map.

5.1 Power entropy vis-a-vis Axiality of multipoles

5.1.1 Full sky analysis

Here we study statistical anisotropy of the multipoles in PLANCK E -mode polarization map as obtained from full sky Stokes Q/U CMB maps, derived using COMMANDER and NILC cleaning procedures. The Power entropy, S_p , is computed for each multipole in the chosen multipole range $l = 40 - 150$ from the E -mode polarization maps using Eq. (14). The statistical significance of the Power entropy values thus computed from data are studied using 4000 isotropic random CMB E -mode polarization maps that are appropriately filtered (see Eq. (19)) and added with the noise proxy of the data i.e., half-ring half-difference (HRHD) maps of respective component separation methods. Fig. (2) shows the null distribution of Power entropy for the multipoles in the range $l = 40 - 150$, but at an interval of 10 multipoles i.e., for $l = 40, 50, 60 \dots 150$ for brevity. The two histograms in each plot corresponding to the two data sets (component separation maps) used in the analysis and the two vertical lines indicate the respective data values.

In Fig. (3), we show the Power entropy, S_p , values from data for all the multipoles in the range $l = 40 - 150$. The data values are denoted by *red* and *blue* points, where the blue ones correspond to those multipoles whose Power entropy has a probability of $P \leq 5\%$. Also plotted are 90%, 95% and 99% confidence contours of distribution of Power entropy, as obtained using 4000 simulations, with a *magenta* line, *gold* and *cyan* colour bands respectively. The rugged nature of the distribution can be understood from the fact that we

Map	Multipoles	Cumulative Probability
COMMANDER	52, 57, 60, 65, 76, 92, 95, 97, 146	0.104
NILC	44, 45, 51, 54, 56, 60, 66, 78, 81, 90, 92, 95, 97, 98, 100, 102, 104, 108, 122, 143, 147	1.390×10^{-7}

Table 1. List of multipoles with probability $P \leq 0.05$ for Power entropy from PLANCK’s full sky cleaned E -mode polarization maps as indicated are given in *second* column. The cumulative probability for finding the observed number of statistically anisotropic modes in individual cleaned maps with $P \leq 0.05$ are furnished in the *third* column.

used the same HRHD map in our simulations to mimic the data noise levels.

The list of multipoles which are found to be statistically anisotropic are listed in second column of Table (1) corresponding to each PLANCK component separated polarization map we used. We find that there are $k_{data} = 9$ and 21 number of multipoles which have $P \leq 0.05$ in the range we analyzed in COMMANDER and NILC E -mode polarization maps respectively. The total number of independent trials for the range $40 \leq l \leq 150$ is 111. Following Eq. (18), we can compute the cumulative probability of finding k_{data} or more instances of statistically anisotropic modes among all the modes analyzed. Note that we defined the criteria of pass or fail with a reference probability of $\mathbb{P} = 0.05$. Thus, from the binomial distribution, the *cumulative* probability, $f(k \geq k_{data} | 111, \mathbb{P} = 0.05)$ are found to be 0.104 and 1.390×10^{-7} , respectively for COMMANDER and NILC maps. These are also listed in Table (1), in the *third* column. As is obvious, we find that the cumulative probability for the observed Power entropy in NILC E -mode polarization map is very small compared to that of COMMANDER map. This is so owing to more number of multipoles being axial in NILC map at the level of 2σ or more than in COMMANDER map.

From Fig. (3) or Table (1) we see that there is a significant indication of violation of statistical isotropy in the PLANCK polarization maps we studied. One may argue that this may be arising due to residual foregrounds that are potentially present in the cleaned maps. In the next section we will try to minimize the effect of this residual contamination following the procedure described in section 4 and re-evaluate the significances reported here.

5.1.2 Understanding the effect of galactic residuals

In this section, we present the result obtained from the full sky E -mode data polarization maps constructed as discussed in section 4. We first apply the common UPB77 mask on the cleaned PLANCK IQU polarization maps and construct the full sky CMB data IQU maps by filling the masked region with a filtered random CMB realization (Eq. (19) added with HRHD noise map. We then extract full sky E -mode polarization maps from the filled Q/U maps, and use these to study the statistical isotropy of multipoles in the range

Map/Mask	Multipoles	Cumulative Probability
COMMANDER/ UPB77	58, 76, 98, 108, 146	0.656
COMMANDER/ PMCMDR	57, 58, 76, 95, 98, 108, 146	0.320
NILC/ UPB77	45, 51, 54, 56, 60, 78, 81, 84, 92, 95, 98, 108	9.726×10^{-3}
NILC/ PMNILC	56, 60, 66, 78, 84, 90, 92, 95, 104, 108, 122, 149	9.726×10^{-3}

Table 2. Same as Table (1), but for full sky E -polarization maps constructed by filling the potentially contaminated galactic region as defined by various masks (see section 4 for more details). The two component separated polarization maps considered here, were studied using both the individual polarization masks - the PMCMDR and PMNILC masks, as well as the common UPB77 mask shown in Fig. (1). The *second* column lists the anomalous multipoles that are outside the 2σ confidence level, and the *third* column lists the cumulative probabilities for finding the observed number or more of the statistically anisotropic multipoles in the range $l = 40 - 150$, that have a P -value $\leq 5\%$.

$l = 40 - 150$. We also use component separation specific polarization masks *PMCMDR* and *PMNILC* corresponding to COMMANDER and NILC procedures respectively to construct full sky E -mode polarization maps following the same procedure. The exercise is then repeated with these maps to reassess the statistics presented before. As explained in section 4, the data statistic is taken as average value of the statistic derived from 100 such randomly filled full sky COMMANDER and NILC IQU maps. We note that such a filling procedure is expected to reduce any signal of statistical anisotropy if present, because of the randomizing effect of the filling.

The list of multipoles having $P \leq 0.05$ in various cases considered are given in *second* column of Table (2). Now, using the common UPB77 mask for filling, we find that there are only 5 and 12 multipoles having a probability of $P \leq 5\%$ compared to that of simulations for COMMANDER and NILC maps respectively. Similarly, by filling the masked region with the individual masks available with each component separation map (PMCMDR and PMNILC), we find that there are 7 and 12 multipoles with $P \leq 0.05$ for COMMANDER and NILC E -mode polarization maps respectively. Thus applying various masks reveals the (in)stability of anomalous multipoles against galactic cuts and potential foreground contamination. The corresponding cumulative probabilities in various cases are listed in the *third* column of Table (2).

From Table (2), one notices that the cumulative probabilities are larger in the *filled* sky E -mode polarization maps than cleaned *full* sky maps, evidently owing to the decrease in number of anomalous multipoles in the later case.

In Fig. (4), we show the Power entropy values from data in comparison to those derived from simulations. As mentioned earlier in section 4, the observed S_p values for each multipole are obtained as average value of the statistic over 100 random fillings of the data to construct full sky E -mode

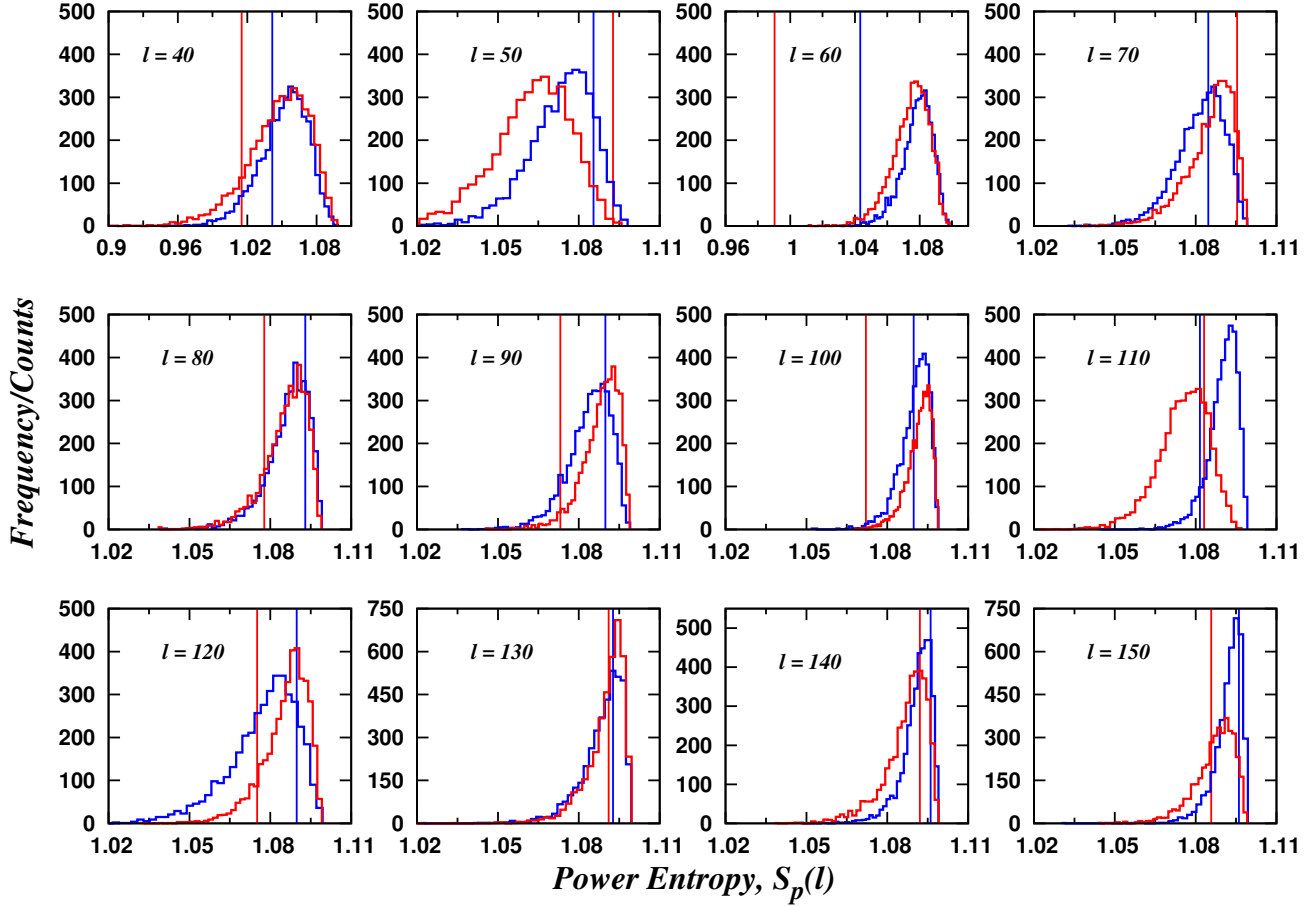


Figure 2. Empirical distribution of Power entropy ‘ S_p ’, obtained from 4000 simulated E -maps with appropriate noise, for the multipole range $40 \leq l \leq 150$, but shown at intervals of 10 multipoles. The *blue* and *red* color histograms in each plot correspond to COMMANDER and NILC simulations. Similarly the vertical lines in respective colors indicate the data value from full sky E -mode polarization maps obtained from COMMANDER and NILC Stokes Q/U maps as provided.

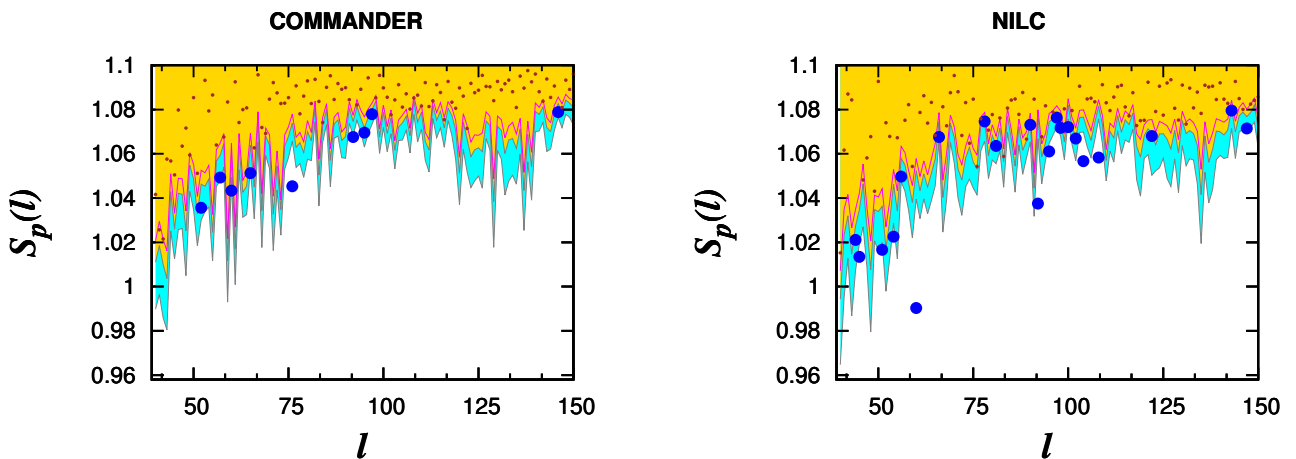


Figure 3. Power entropy (S_p) values from full sky COMMANDER (*left*) and NILC (*right*) E -polarization maps over the range $l = 40-150$ are shown here. The data S_p values in each plot are shown as *red* and *blue* dots, where the *blue* points highlight those multipoles whose Power entropy has a P -value less than 5%. The magenta line, gold and cyan bands represent 90%, 95% and 99% confidence contours estimated from 4000 simulations.

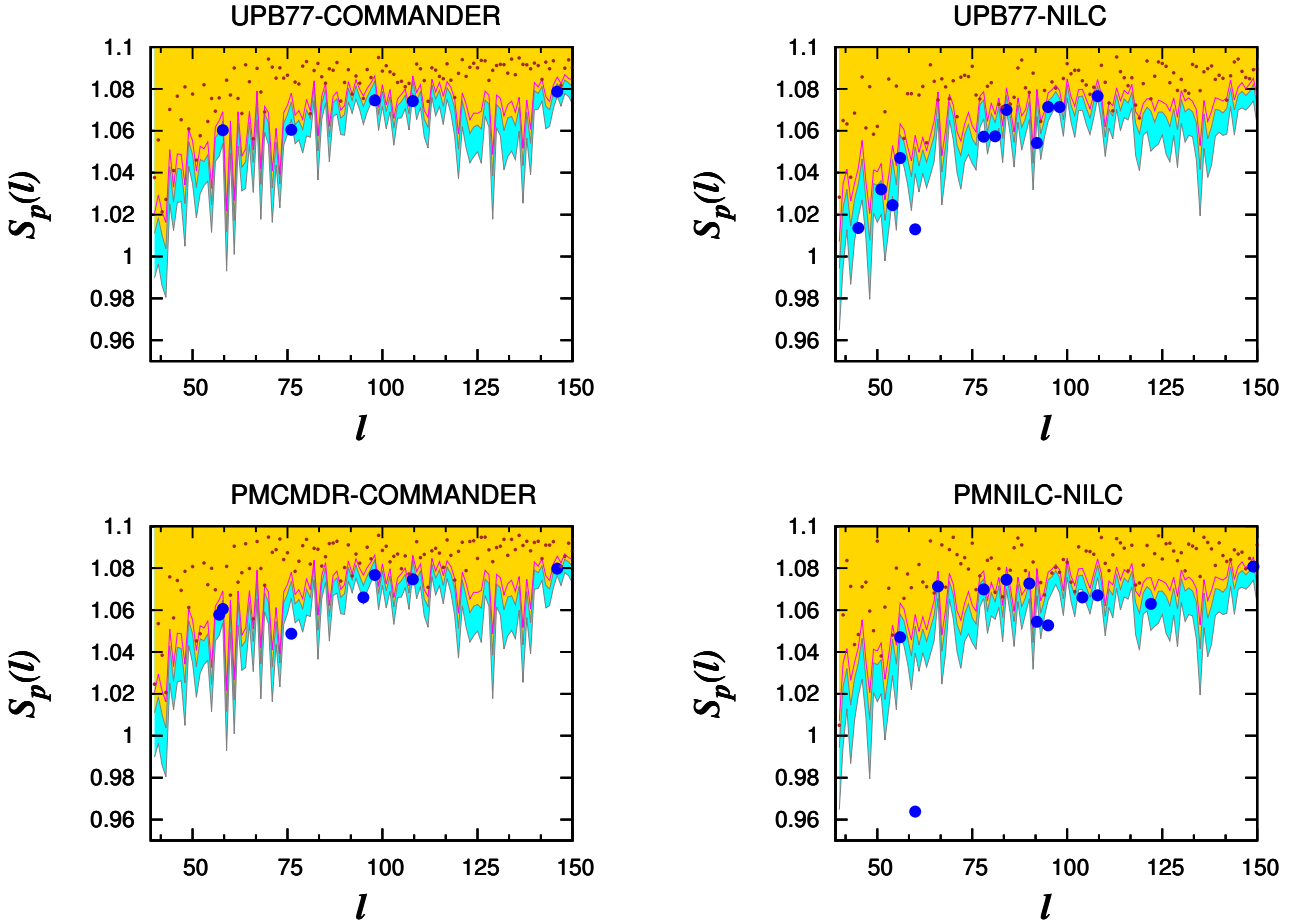


Figure 4. Plotted here are the Power entropy (S_p) values as obtained from full sky PLANCK’s COMMANDER and NILC E -maps constructed after filling the masked sky defined by various polarization masks shown in Fig. (1). The *first* and *second* columns correspond to the Power entropy for the range $l = 40 - 150$ as obtained from COMMANDER and NILC E -polarization maps. The *top* and *bottom* figures in each column correspond to the use of UPB77 common polarization mask and the component separation specific PMCMDR/PMNILC mask on respective cleaned maps. The color coding of data points and confidence contours is same as in Fig. (3).

polarization maps. The contours of 90%, 95% and 99% confidence levels from simulations are shown as *magenta* line, *gold* band, and *cyan* band respectively. The data points are shown as *red* dots, while those which are outside the 2σ contour are denoted by *blue* points. This contour plot neatly highlights various multipoles which are inconsistent with the isotropic predictions. So, we may now say that presence of residual foregrounds indeed had an effect on our isotropy test when full sky polarization maps are used as provided. In both COMMANDER and NILC maps, the number of anomalous multipoles nearly reduced by half when full sky maps are constructed using UPB77 mask. However since noise is dominant in the PLANCK polarization maps, the stability of these modes can only be validated in the future.

5.2 Alignments across multipoles

In this section, we discuss alignments among multipoles in the chosen multipole range using Alignment entropy, S_X , as defined in Eq. (15). We divide the chosen range $l = 40 - 150$ into 10 multipole bins having 11 multipoles per bin. Thus the multipole bins we analyze are $l = 40-50, 51-61, 62-72, 73-83, 84-94, 95-105, 106-116, 117-127, 128-138$ and

$139-149$. The statistic, S_X , is computed for each multipole bin and its significance is estimated using simulations that are generated as discussed in section 4.

5.2.1 Full sky analysis

Here we probe for any coherent alignments across multipoles in E -mode polarization maps as obtained using PLANCK’s full sky Stokes Q/U CMB maps, derived using COMMANDER and NILC cleaning procedures. In each multipole bin of the data maps, Alignment entropy is calculated. The statistical significance of S_X are obtained by comparing the data statistic with 4000 isotropic random CMB E -mode filtered polarization maps added with the noise proxy (HRHD map) of respective component separation methods.

The list of multipole bins and the significance of S_X for these bins are listed in *second* and *third* column of Table (3) respectively. As we can see from that table, the multipole bins $40 - 50, 84 - 94, 95 - 105, 106 - 116, 117 - 127,$ and $139 - 149$ have a P -value ≤ 0.05 for Alignment entropy. We extract the common alignment vector from PEVs for a bundle of multipoles using the Alignment tensor, X , defined in Eq. (16). The common alignment vector is taken as the

Map	Multipole Range	P -value	(l, b)
COMMANDER	40 – 50	< 1/4000	(87°, 27°)
	51 – 61	0.19	-
	62 – 72	0.23	-
	73 – 83	0.15	-
	84 – 94	< 1/4000	(95°, 19°)
	95 – 105	< 1/4000	(96°, 30°)
	106 – 116	0.013	(75°, 18°)
	117 – 127	0.002	(103°, 33°)
	128 – 138	0.424	-
	139 – 149	0.021	(90°, 26°)
NILC	40 – 50	0.008	(87°, 24°)
	51 – 61	0.092	-
	62 – 72	0.083	-
	73 – 83	0.001	(99°, 29°)
	84 – 94	< 1/4000	(93°, 31°)
	95 – 105	< 1/4000	(95°, 29°)
	106 – 116	< 1/4000	(82°, 21°)
	117 – 127	0.02	(96°, 36°)
	128 – 138	0.12	-
	139 – 149	0.002	(98°, 46°)

Table 3. Significance of Alignment entropy (S_X) and direction of common alignment axis obtained using Alignment tensor (X) corresponding to various multipole bins of the cleaned E -mode polarization maps, derived from full sky Stokes Q/U COMMANDER and NILC maps, are listed here. The range $l = 40 - 150$ is divided into 10 multipole bins. The P -value of S_X for various bins are given in the *third* column. Where none of the simulations yield a value less than the data statistic, it's significance is listed as < 1/4000. The direction of the common alignment axis for those bins whose P -value is ≤ 0.05 are given in the *fourth* column.

eigenvector corresponding to the largest eigenvalue of the Alignment tensor matrix. The common alignment vector direction of those bins in galactic co-ordinates, (l, b) , having P -value $\leq 5\%$ for S_X are also listed in Table (3), in the *fourth* column. We notice that these vectors almost lie in the galactic region. The effect of the presence of residual contamination on these vectors will be assessed in the next section. For ease of comparison, we also show the observed significances of S_X in various multipole bins from full sky COMMANDER and NILC E -maps in Fig. (5). The Alignment entropy from data corresponding to some of the multipole bins was always smaller than the simulations. Therefore we denoted those histogram bars with a triangle at the top to indicate that the significance of data statistic is < 1/4000.

5.2.2 Filled sky analysis

In order to understand the likely effect of residual contamination in the PLANCK full sky CMB polarization maps on our collective alignments' study, here we use filled E -mode data polarization map, generated as discussed in section 4. The common *UPB77* mask is first applied on the cleaned PLANCK's COMMANDER and NILC IQU maps and the statistic S_X is obtained as mean value of the same quantity from filled IQU maps constructed using 100 random realizations of CMB with HRHD noise proxy to fill the masked portion in the data maps. The filling is also performed using the other two polarization masks shown in Fig. (1), viz., the component specific *PMCMDR* and *PMNILC* masks corresponding to COMMANDER and NILC foreground cleaning schemes. The statistical significance of the observed

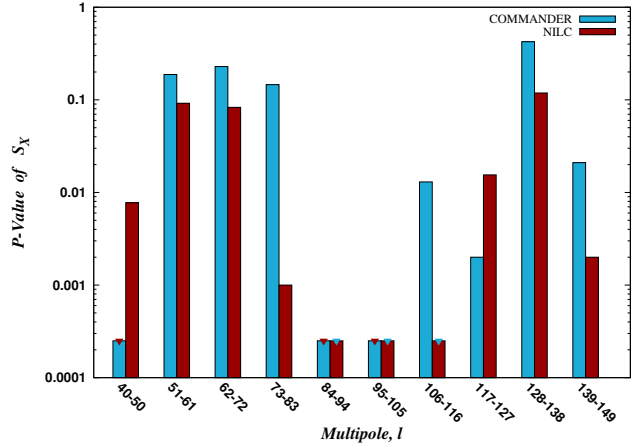


Figure 5. P -values of Alignment entropy, S_X , corresponding to various multipole bins in the range $l = 40 - 150$ (divided into 10 bin) are plotted here. The two bars at each multipole bin as indicated correspond to the significances of Alignment entropy for that bin from CMB E -mode polarization maps derived from full sky Stokes Q/U COMMANDER and NILC maps. Those histogram bars which have a triangle at the top, denote a significance < 1/4000.

value of Alignment entropy is studied using 4000 CMB E -mode realizations with noise.

The list of multipole bins and the significance of S_X from these bins are given in Table (4). Now, we find that the multipole bins, $l = 40 - 50, 84 - 94, 95 - 105, 106 - 116,$ and $139 - 149$ have $P \leq 0.05$ using the *UPB77* mask, and $l = 40 - 50, 84 - 94, 95 - 105, 106 - 116, 117 - 127,$ and $139 - 149$ multipole bins have P -value ≤ 0.05 with *PMCMDR* mask on COMMANDER polarization map. Similarly for NILC polarization map, the multipole bins that are anomalous at 2σ level are $l = 40 - 50, 51 - 61, 84 - 94, 95 - 105, 106 - 116, 117 - 127, 128 - 138,$ and $139 - 149$ when *UPB77* mask was used, and $l = 40 - 50, 51 - 61, 73 - 83, 84 - 94, 95 - 105, 106 - 116, 117 - 127, 128 - 138,$ and $139 - 149$ bins when *PMNILC* mask was used.

The collective alignment vector direction for various bins obtained using Alignment tensor, X , (Eq. (16)) which are found to have a P -value $\leq 5\%$ for S_X are tabulated in the last column of Table (4). Even in this case, we see that these collective alignment vectors lie closer to the galactic region. Hence these modes found to be anomalous may still be affected by residual foreground bias. In Fig. (6), the P -values of S_X found in the filled sky case for various multipole bins and masks used are shown as histograms for ready comparison.

6 CONCLUSION

In the present work, we studied violation of isotropy of various modes that are available in the cleaned CMB polarization maps from PLANCK full mission data release. Specifically we scrutinized the multipole range $l = 40 - 150$ of the E -mode CMB maps derived using the COMMANDER and NILC Q/U polarization maps. We applied our symmetry based *Power tensor* method to test statistical (an)isotropy

Map/Mask	Multipole bin	P -value	(l, b)
COMMANDER/ UPB77	40 – 50	0.0005	$(85^\circ, 24^\circ)$
	51 – 61	0.106	-
	62 – 72	0.273	-
	73 – 83	0.056	-
	84 – 94	0.002	$(91^\circ, 22^\circ)$
	95 – 105	0.025	$(98^\circ, 47^\circ)$
	106 – 116	0.014	$(72^\circ, 29^\circ)$
	117 – 127	0.064	-
	128 – 138	0.123	-
139 – 149	0.012	$(88^\circ, 34^\circ)$	
COMMANDER/ PMCMDBR	40 – 50	0.0005	$(85^\circ, 31^\circ)$
	51 – 61	0.055	-
	62 – 72	0.13	-
	73 – 83	0.58	-
	84 – 94	0.0013	$(89^\circ, 27^\circ)$
	95 – 105	0.007	$(98^\circ, 40^\circ)$
	106 – 116	0.0008	$(72^\circ, 28^\circ)$
	117 – 127	0.05	-
	128 – 138	0.156	-
	139 – 149	0.0234	$(91^\circ, 33^\circ)$
	NILC/ UPB77	40 – 50	$< 1/4000$
51 – 61		0.007	$(101^\circ, 35^\circ)$
62 – 72		0.342	-
73 – 83		0.137	-
84 – 94		$< 1/4000$	$(92^\circ, 16^\circ)$
95 – 105		0.0003	$(100^\circ, 36^\circ)$
106 – 116		$< 1/4000$	$(84^\circ, 27^\circ)$
117 – 127		0.002	$(99^\circ, 25^\circ)$
128 – 138		0.002	$(92^\circ, 38^\circ)$
139 – 149	0.002	$(90^\circ, 34^\circ)$	
NILC/ PMNILC	40 – 50	0.003	$(90^\circ, 26^\circ)$
	51 – 61	0.002	$(102^\circ, 38^\circ)$
	62 – 72	0.47	-
	73 – 83	0.03	$(105^\circ, 28^\circ)$
	84 – 94	$< 1/4000$	$(97^\circ, 29^\circ)$
	95 – 105	$< 1/4000$	$(100^\circ, 31^\circ)$
	106 – 116	$< 1/4000$	$(80^\circ, 20^\circ)$
	117 – 127	0.001	$(98^\circ, 27^\circ)$
	128 – 138	0.08	-
139 – 149	0.002	$(99^\circ, 43^\circ)$	

Table 4. Same as Table (3), but the significances of S_X and direction of common alignment axis for various bins correspond to filled sky polarization maps as indicated (see text for details). The P -values are listed in *third* column and the common alignment vectors for only those bins whose Alignment entropy, S_X , is found to be anomalous at 2σ level are listed in *fourth* column.

of these maps. A set of 4000 simulations were generated using the theoretical angular power spectrum obtained using the best fit cosmological parameters from PLANCK 2015 release in the CAMB software package. These realizations were smoothed with appropriate beam window function, and filtered using a high-pass cosine filter to retain only those modes in simulations, that are currently made available in the data. The half-ring half-difference (HRHD) maps of respective component separation methods were taken as noise proxy, and added with the smoothed, filtered E -mode random CMB realizations to generate mock observed maps.

In order to understand the effect of potential bias due to residual foregrounds in the full sky cleaned polarization maps on our isotropy studies, we generated another set of full sky maps where we filled part of the sky that is omitted by the UPB77 polarization mask with 100 appropriate random CMB maps with noise. All the statistics computed in the filled sky case are taken as average value of the same quantity over these 100 *filled* full sky E -mode data maps. We also used the individual polarization masks from COMMANDER

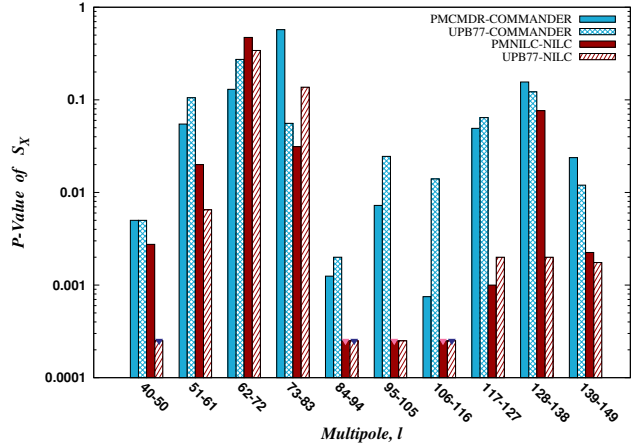


Figure 6. Same as Fig. (5), but for the filled sky CMB polarization maps viz, COMMANDER E -map by filling the masked region defined by the common UPB77 and PMCMDBR masks, and the NILC E -map where the inside of the masking portion defined by UPB77 and PMNILC masks is filled, using a random CMB realization and HRHD noise proxy. The data statistic is computed as average of the same quantity extracted from 100 such random fillings of the data, which is then used to compute significances. Here also, those multipole bins for a given component separation map/mask combination where the significance was found to be $< 1/4000$, their histogram bar is plotted with a triangle at the top.

and NILC foreground removal methods. We reiterate that the filling procedure we employed is only expected to lower any signal of statistical anisotropy if present, because of the randomizing nature of the filling process.

We note the following observations. The number of anomalous multipoles that indicate isotropy violation at the level of 2σ in the full sky COMMANDER and NILC polarization maps are found to be 9 and 21 respectively. However when this same range $l = 40 - 150$ is analyzed using filled sky maps constructed using the conservative UPB77 polarization mask, the number of anomalous modes have reduced to nearly half. The number remains albeit the same when component specific polarization masks are used. Thus we may say that the galactic residuals indeed have an effect on our test of isotropy of various multipoles. It is interesting to note that the number of anomalous multipoles with P -value ≤ 0.05 are more in NILC CMB E -map than in the COMMANDER map. This observation is particularly interesting given that the recovered CMB signal using NILC procedure is supposed to be very reliable over a much larger fraction of the sky than the COMMANDER map. The respective masking fractions of COMMANDER and NILC polarization masks are $\approx 83\%$ and 96% . The effective probability of finding the observed number of statistically anisotropic modes in the range $l = 40 - 150$ in NILC map using various masks is correspondingly low.

We then studied alignments across multipoles using *Alignment entropy* over the chosen range $l = 40 - 150$, divided into 10 blocks with 11 multipole per bin. Here also we analyzed full sky as well as filled sky maps for coherent alignments across multipoles using 4000 simulations. All three polarization masks considered in the preceding anal-

ysis were applied to data E -maps to understand any foreground biases. We find a tentative evidence for collective alignment in some of the multipole blocks. However, we also found that the direction of these common alignment axes lie closer to the galactic plane in both full sky and filled sky cases. Hence the effect of galactic bias, even after filling the potentially contaminated regions, may still be significant. In these alignment tests as well, we find that more number of multipole bins are anomalous in NILC map compared to COMMANDER CMB E -map.

Thus, the modes currently available in the polarization maps we analyzed appear to be sensitive to various galactic cuts. Further, the number and actual modes that are anomalous change, by applying different masks with few common multipoles surviving among them. These multipoles may also be effected by noise, given that the noise levels are significant in PLANCK polarization measurements. In light of these, an analysis of improved polarization maps from PLANCK in a future data release can only confirm our findings. In this work, however, we didn't make any attempt to identify the exact cause of the observed isotropy violation in polarization maps.

ACKNOWLEDGEMENTS

We thank the anonymous referee for a careful reading of our manuscript and the suggestions made, which greatly helped in improving clarity and overall presentation of our work. Some of the results in the current work were derived using the publicly available HEALPix package¹. We also acknowledge the use of CAMB², a freely available Boltzmann solver for CMB anisotropies. Part of the results presented here are based on observations obtained with PLANCK³, an ESA science mission with instruments and contributions directly funded by ESA Member States, NASA, and Canada.

REFERENCES

- Aiola S., Wang B., Kosowsky A., Kahnishvili T., Firouzjahi H., 2015, *Phys. Rev. D*, **92**, 063008
- Akrami Y., Fantaye Y., Shafieloo A., Eriksen H. K., Hansen F. K., Banday A. J., Górski K. M., 2014, *Astrophysical Journal Letters*, **784**, L42
- Aluri P. K., Jain P., 2012, *Mon. Not. R. Astron. Soc.*, **419**, 3378
- Aluri P. K., Rath P. K., 2016, *Mon. Not. R. Astron. Soc.*, **458**, 4269
- Aluri P. K., Ralston J. P., Weltman A., 2017, *Mon. Not. R. Astron. Soc.*, **472**, 2410
- Bennett C. L., Hill R. S., Hinshaw G., et al., 2011, *Astrophysical Journal*, **192**, 17
- Bielewicz P., Eriksen H. K., Banday A. J., Gorski K. M., Lilje P. B., 2005, *Astrophysical Journal*, **635**, 750
- Birch P., 1982, *Nature*, **298**, 451
- Copi C. J., Huterer D., Starkman G. D., 2004, *Phys. Rev. D*, **70**, 043515
- Copi C. J., Huterer D., Schwarz D. J., Starkman G. D., 2006, *Mon. Not. R. Astron. Soc.*, **367**, 79
- Cruz M., Martínez-González E., Vielva P., Cayón L., 2005, *Mon. Not. R. Astron. Soc.*, **356**, 29
- Cruz M., Tucci M., Martínez-González E., Vielva P., 2006, *Mon. Not. R. Astron. Soc.*, **369**, 57
- Cruz M., Martínez-González E., Vielva P., Diego J. M., Hobson M., Turok N., 2008, *Mon. Not. R. Astron. Soc.*, **390**, 913
- de Oliveira-Costa A., Tegmark M., Zaldarriaga M., Hamilton A., 2004, *Phys. Rev. D*, **69**, 063516
- Eriksen H. K., Hansen F. K., Banday A. J., Gorski K. M., Lilje P. B., 2004, *Astrophysical Journal*, **605**, 14
- Gorski K., Hivon E., Banday A. J., Wandelt B. D., Hansen F. K., Reinecke M., Bartelmann M., 2005, *Astrophysical Journal*, **622**, 759
- Hajian A., Souradeep T., 2003, *Astrophysical Journal*, **597**, L5
- Hajian A., Souradeep T., 2006, *Phys. Rev. D*, **74**, 123521
- Hansen F. K., Banday A. J., Gorski K. M., Eriksen H. K., Lilje P. B., 2009, *Astrophysical Journal*, **704**, 1448
- Hanson D., Lewis A., 2009, *Phys. Rev. D*, **80**, 063004
- Hoftuft J., Eriksen H. K., Banday A. J., Gorski K. M., Hansen F. K., Lilje P. B., 2009, *Astrophysical Journal*, **699**, 985
- Howlett C., Lewis A., Hall A., Challinor A., 2012, *Journal of Cosmology and Astroparticle Physics*, **4**, 027
- Hutsemekers D., 1998, *Astronomy and Astrophysics*, **332**, 410
- Hutsemekers D., Lamy H., 2001, *Astronomy and Astrophysics*, **367**, 381
- Jain P., Ralston J. P., 1999, *Modern Physics Letters A*, **14**, 417
- Jain P., Narain G., Sarala S., 2004, *Mon. Not. R. Astron. Soc.*, **347**, 394
- Kim J., Naselsky P., 2010, *Astrophysical Journal Letters*, **714**, L265
- Kim J., Naselsky P., 2011, *Astrophysical Journal*, **739**, 79
- Land K., Magueijo J., 2005, *Phys. Rev. D*, **378**, 153
- Lewis A., Challinor A., Lasenby A., 2000, *Astrophysical Journal*, **538**, 473
- Nadathur S., Lavinto M., Hotchkiss S., Räsänen S., 2014, *Phys. Rev. D*, **90**, 103510
- Naselsky P. D., Christensen P. R., Coles P., Verkhodanov O. V., Novikov D. I. Kim J., 2010, *Astrophys. Bull.*, **65**, 101
- Planck Collaboration XXIII, 2013, *Astronomy and Astrophysics*, **571**, A23
- Planck Collaboration IX, 2016, *Astronomy and Astrophysics*, **594**, A9
- Planck Collaboration XI, 2016, *Astronomy and Astrophysics*, **594**, A11
- Planck Collaboration XIII, 2016, *Astronomy and Astrophysics*, **594**, A13
- Planck Collaboration XVI, 2016, *Astronomy and Astrophysics*, **594**, A16
- Prunet S., Uzan J. P., Bernardeau F., Brunier T., 2005, *Phys. Rev. D*, **71**, 083508
- Ralston J. P., Jain P., 2004, *International Journal of Modern Physics D*, **13**, 1857
- Rath P. K., Jain P., 2013, *Journal of Cosmology and Astroparticle Physics*, **12**, 14
- Rath P. K., Mudholkar T., Jain P., Aluri P. K., Panda S., 2013, *Journal of Cosmology and Astroparticle Physics*, **4**, 7
- Rath P. K., Aluri P. K., Jain P., 2015, *Phys. Rev. D*, **91**, 023515
- Rath P. K., Samal P. K., 2015, *Modern Physics Letters A*, **30**, 1550131
- Samal P. K., Saha R., Jain P., Ralston J. P., 2008, *Mon. Not. R. Astron. Soc.*, **385**, 1718
- Samal P. K., Saha R., Jain P., Ralston J. P., 2009, *Mon. Not. R. Astron. Soc.*, **396**, 511
- Samal P. K., Saha R., Delabrouille J., Prunet S., Jain P., Souradeep T., 2010, *Astrophysical Journal*, **714**, 840
- Schwarz D. J., Starkman G. D., Huterer D., Copi C. J., 2004, *Physical Review Letters*, **93**, 221301

¹ <https://healpix.jpl.nasa.gov/>

² <http://camb.info/>

³ <http://www.esa.int/Planck>

Vielva P., Martínez-González E., Barreiro R. B., Sanz J. L., Cayón L., 2004, [Astrophysical Journal](#), 609, 22
Zaldarriaga M., Seljak U., 1997, [Phys. Rev. D](#), 55, 1830
Zhao W., 2013, [Mon. Not. R. Astron. Soc.](#), 433, 3498
Zhao W., 2014, [Phys. Rev. D](#), 89, 023010

This paper has been typeset from a $\text{\TeX}/\text{\LaTeX}$ file prepared by the author.